Malvinas Current at 40°S–41°S: first assessment of temperature and salinity temporal variability

Guillermina Paniagua, Martin Saraceno, Alberto R. Piola, Raúl Guerrero, Christine Provost, Ramiro Ferrari, Loreley Lago, Camila Artana

AGU100 ADVANCING EARTH AND SPACE SCIENCE

JGR

Journal of Geophysical Research: Oceans

RESEARCH ARTICLE

10.1029/2017JC013666

Malvinas Current at 40°S–41°S: First Assessment of Temperature and Salinity Temporal Variability

Guillermina F. Paniagua[1,2,3], Martin Saraceno[1,2,3], Alberto R. Piola[2,3,4], Raúl Guerrero[5], Christine Provost[6], Ramiro Ferrari[1,3], Loreley S. Lago[2,3,5], and Camila I. Artana[6]

[1]Centro de Investigaciones del Mar y la Atmósfera (CIMA/CONICET-UBA), Ciudad Autónoma de Buenos Aires, Argentina, [2]Departamento de Ciencias de la Atmósfera y los Océanos FCEN Universidad de Buenos Aires, Buenos Aires, Argentina, [3]Unidad Mixta Internacional-Instituto Franco-Argentino para el Estudio del Clima y sus Impactos (UMI-IFAECI/CNRS-CONICET-UBA), Buenos Aires, Argentina, [4]Departamento de Oceanografía, Naval, de Servicio Hidrografía (SHN), Buenos Aires, Argentina, [5]Instituto Nacional de Investigación y Desarrollo Pesquero, Mar del Plata, Argentina, [6]Laboratoire d'Océanographie et du Climat: Experimentation et Approches Numériques (LOCEAN) UMR 7159, Paris, Francia

Abstract The temporal variability of 11 months of in situ velocity, temperature, and salinity data collected at five moorings deployed at 40°S–41°S across the shelf-break in the Southwestern Atlantic is analyzed. Two distinct regimes characterized by strong and weak along-slope velocities are present. During the strong regime the Malvinas Current flows northward through the moorings while during the nearly 5 months long weak regime reversals of the along-slope velocities are frequently observed. Comparison with the previous in situ time series obtained in the same region shows that such an extended period of weak flow has not been previously observed. During the weak regime, Sub-Antarctic Mode Water is observed over the 1,800 m isobath at an average depth of 500 m. Water masses occupying the upper 1,600 m during the strong regime deepen and shift eastward during the weak period. Satellite geostrophic velocities and sea surface temperature clearly show that the weak regime is due to a deflection to the east of the Malvinas Current, upstream of the mooring position. Analysis of the vertical structure of the currents indicate that during the weak regime the flow weakens mostly at the surface and presents a very small vertical shear. In contrast, during the strong regime currents are surface-intensified. The change in the structure of the currents at the mooring location impacts the relationship between in situ and altimetry-derived currents: during the weak regime altimetry adequately represents (rmsd 12 cm/s) in situ currents in the whole water column, while during strong regime rmsd are larger than 15 cm/s below 600 m depth.

Key Points:
- Malvinas Current at 40°S–41°S shifts between two regimes: the strong (weak) regime has along-slope velocities that are large (weak) and surface-intensified (almost zero-vertical shear)
- The weak regime is due to a deflection of the Malvinas Current to the east, upstream of the mooring site
- A large shift of the structure of the water masses accompany the along-slope velocity change: all water masses present in the upper 1,600 m sink and shift eastward during the weak regime

Supporting Information:
- Figure S1–S12

Correspondence to:
G. F. Paniagua,
guillermina.paniagua@cima.fcen.uba.ar

Citation:
Paniagua, G. F., Saraceno, M., Piola, A. R., Guerrero, R., Provost, C., Ferrari, R., et al. (2018). Malvinas Current at 40°S–41°S: First assessment of temperature and salinity temporal variability. *Journal of Geophysical Research: Oceans*, *123*, 5323–5340. https://doi.org/10.1029/2017JC013666

Received 3 DEC 2017
Accepted 14 MAY 2018
Accepted article online 29 MAY 2018
Published online 8 AUG 2018

1. Introduction

The Malvinas Current (MC) is the northernmost extension of the Antarctic Circumpolar Current that carries cold and nutrient-rich waters to subtropical latitudes up to 38°S, with significant biological and biogeochemical impact in the neighboring ocean. Satellite-derived color images show chlorophyll-a concentrations as large as those present on eastern boundary upwelling systems at the shelf-break (Romero et al., 2006; Saraceno et al., 2005). This productivity spreads through the food-web, reaching top predators and leading to significant fisheries (Acha et al., 2004). The interaction of the MC with the sloping bottom is presumably responsible for sustaining upwelling along the shelf-break (Matano & Palma, 2008). Numerical and analytical models indicate that the upwelling intensity is modulated by the MC transport (Matano & Palma, 2008; Miller et al., 2011). However, the nature of the shelf-slope interactions is still poorly understood: little is known about the influence of the MC dynamics on the maintenance of the extremely productive region over the shelf-break, on how the nutrients supplied by the MC are capitalized over the Patagonian Continental Shelf (PCS) and how and if these fluxes depend on the continental shelf and slope circulation. To a large extent, the scarcity of in situ observations is responsible for this poor understanding. The first current time series data on the MC were collected on 5 moorings deployed from December 1993 to June 1995 at 41°S along TOPEX-POSEIDON track 26 (Figure 1) totalizing 17 current meters (Vivier & Provost, 1999a) as part of the World Ocean Circulation Experiment (WOCE). Based on these observations, the flow of the MC is revealed as an equivalent-barotropic structure due to the weak stratification and the steep topography (Vivier & Provost, 1999b). A reduced array of three moorings totalizing 6 current meters, 8 years later, provided new

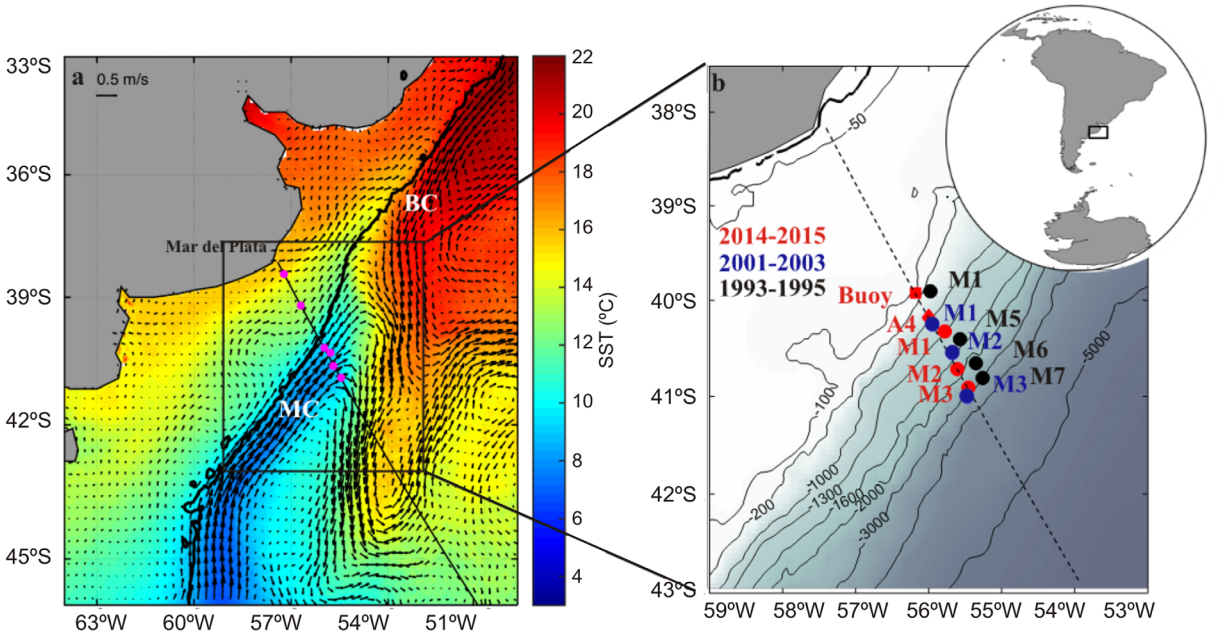

Figure 1. (a) Mean sea surface temperature (MODIS 4 km resolution) and satellite altimetry velocities between December 2014 and November 2015. Magenta dots represent position of the moorings of the CASSIS project. (b) Location of the current meter moorings deployed in 1993–1995 (magenta), 2001–2003 (blue) and in 2014–2015 (red). Tall moorings, the oceanographic buoy, and upward-looking ADCPs are indicated with circles, squares, and diamonds, respectively. Satellite altimetry Jason track #26 (blue dashed line) and isobaths (black contours) are also indicated. Bottom topography isolines mark the 50, 100, 200, 1,000, 1,300, 1,600, 2,000, 3,000, 4,000, and 5,000 m isobaths (GEBCO; IOC, 2003).

information on the core of the MC above the 1,010 m isobath, where a mooring had been previously lost, and means and statistics that were coherent with the first deployment (Spadone & Provost, 2009). The CASSIS project (www.cima.fcen.uba.ar/malvinascurrent) deployed 16 moorings along two transects that crossed at the same time the PCS and shelf-break. In this work, data recovered from instruments deployed in the northernmost transect over the shelf-break (Figure 1) are analyzed. CASSIS moorings were deployed on the continental slope at the same position, where instruments were deployed in the past, but for the first time, temperature and conductivity sensors at different water levels were deployed and allowed to study the structure of the water masses in conjunction with the currents. The analysis of the spatiotemporal variability of the water masses is particularly important in this region: the MC is the unique current in the southern hemisphere that carries sub-Antarctic waters to latitudes as low as 38°S. The MC contributes in this way to the cold branch of the thermohaline circulation, being a major player to regulate the climate of the Earth (Garzoli & Matano, 2011).

Different water masses characterize the MC on the continental slope in the Southwestern Atlantic. Because of its sub-Antarctic origin, the upper layer is substantially cold (potential temperature <15°C) and fresh (salinity <34.2) with a density range of 25.5–27.0 kg m^{-3} (Gordon, 1981). South of 38°S, fresh Sub-Antarctic Surface Water (SASW) is advected northward along the continental slope by the MC, where it converges with the warm and salty subtropical waters carried poleward by the Brazil Current (BC). The region where the two waters masses collide is usually referred to as the Brazil-Malvinas Confluence (BMC). The MC veers southward after meeting the BC at 38°S. At intermediate depths, the MC carries newly formed South Atlantic Mode Water (SAMW; McCartney, 1977, 1982) and Antarctic Intermediate Water (AAIW, Piola & Gordon, 1989). The SAMW is formed in deep winter convection along the Sub-Antarctic Zone of the northern Drake Passage (McCartney, 1977, 1982; Piola & Gordon, 1989; Piola & Matano, 2001; Talley, 1996). The SAMW is subducted into the subtropical thermocline and is warm and salty compared to the Antarctic Intermediate Water (AAIW) that is located underneath. Indeed, the SAMW is the primary precursor of the AAIW (Maamaatuaiahutapu et al., 1994; Piola & Gordon, 1989). The AAIW that originates from a surface region of the circumpolar layer in the South Atlantic, especially in the northern Drake Passage and the MC loop, can be recognized by a subsurface oxygen maximum and a S minimum ($S<34.3$) (Stramma & England, 1999). South of the BMC, the AAIW/SAMW are fresher ($S<34.1$) than within the BC. The temperature of the core of

the AAIW increases from 3°C, in the Drake Passage, to 3.5°C at 40°S (Piola & Matano, 2001). In the Drake Passage below 800–1,000 m, the Circumpolar Deep Water (CDW) is the deepest water mass of the upper ocean. As the northern branch of the ACC veers northward downstream of Drake Passage the less dense fraction of CDW flows northward within the MC and is identified by a dissolved oxygen minimum. The denser fraction of CDW (or Lower CDW, LCDW) lies between 1,700 and 3,500 m in the BMC region (Piola & Matano, 2001). At 40°S, the lightest portion of the CDW is the Upper Circumpolar Deep Water (UCDW) that is characterized by temperatures lower than 2.9°C and is located approximately at 1,400 m deep.

The above description of water masses is based on classical hydrographic observations. While classical hydrographic observations have great resolution in the vertical, they only allow a description of the water masses at the time of observation. In the vicinity of dynamically active regions as the BMC snapshots so obtained might differ greatly. To assess the time variability of the water masses, tall moorings with temperature and conductivity sensors at different water levels as the one analyzed in this work are therefore useful to understand the time variability at the expense of vertical resolution. This study shows the first assessment of simultaneous temperature, salinity, and current meters records in the region and discuss their temporal variability.

In what follows a description of the data and methods used is provided (section 2). Results obtained are described in section 3 and discussed in section 4, where main findings are highlighted.

2. Data and Methods

Eight mooring arrays were deployed in December 2014 (Figure 1a and Table 1), as part of the French-Argentine CASSIS project using the offshore rescue vessel SB-15 Tango and R/V Puerto Deseado. In the following subsections, the mooring array is described in section 2.1; satellite data used to provide a regional scope of the in situ data are detailed in section 2.2; the methods used for data analysis are explained in section 2.3.

2.1. In Situ Data

2.1.1. Data From the CASSIS Project

The five-mooring array deployed on the shelf-break was located below Jason-2 track #26 between 200 and 3,400 m and between 40°S and 41°S (Figure 1 and Table 1). In the deepest portion of the shelf-break three tall moorings (M1, M2, and M3) comprised 11 current meters (four AANDERAA RCM-8 and seven Aquadopp Profiler) and seven conductivity-temperature (CT) sensors (SBE 37). At 1,010 m depth a bottom mooring (A4) was equipped with an upward-looking RDI Workhorse Long Ranger 75 kHz acoustic Doppler current profiler (ADCP), a bottom pressure recorder (BPR, SBE 53), and a CT sensor (SBE 37). Finally, at 200 m depth, an oceanographic buoy equipped with six CT (SBE 37) sensors installed in the upper 100 m of the water column, a hull-mounted downward-looking Nortek Continental 190 kHz ADCP and meteorological sensors was moored. Figure 2 summarizes the instrument depth and location within each mooring. Hereafter instruments in the tall moorings are labeled Mij, where i represents the mooring number and j stands for the position within the mooring from the surface downward (Figure 2). Potential temperature (θ) was computed for all CT sensors following Bryden (1973).

All instruments moored in the oceanographic buoy and on the tall moorings M1 and M2 recorded hourly data. Current meters on M3 stored data every half hour. On A4, the ADCP was configured to record data every 3 h, the BPR every 15 min and the CT sensors every hour. The sampling frequency is different between instruments because we decided to optimize the number of samples to be collected considering battery consumption, memory capacity, and the aimed duration of the experiment (1 year).

Between 18 and 20 November 2015, A4, M1, M2, and M3 were recovered. All instruments, except a CT sensor on M1, produced 338 days of uninterrupted high-quality data on A4, M1, and M2. Unfortunately, this was not the case for M3 and the oceanographic buoy. Instruments on M3 failed prematurely: after 42 days M31 stopped measuring, whereas deeper current meters recorded data for 5 days only. The ADCP on the oceanographic buoy stopped working the 31 December

Table 1
Position of the Moorings

Mooring name	Latitude (°S)	Longitude (°W)
Buoy	39.9	56.2
A4	40.2	55.9
M1	40.4	55.8
M2	40.6	55.7
M3	40.9	55.5

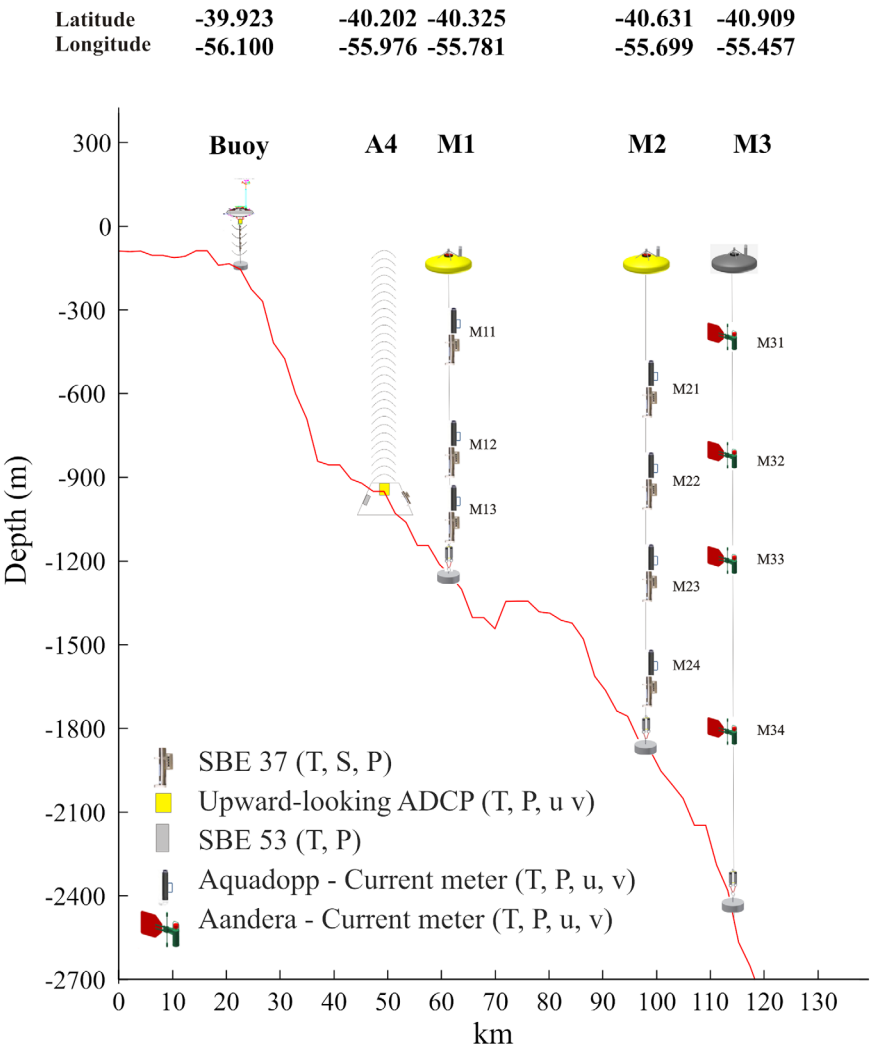

Figure 2. Vertical distribution and position of the instruments along mooring lines deployed in 2014–2015 over the shelf-break. Variables measured by each type of instrument are indicated in the legend. The oceanographic buoy was the only mooring with a surface buoy that transmitted data on real time. It was deployed at 200 m depth and had six SBE 37 to measure T and S in the water column. On the hull, it has a downward-looking ADCP and a meteorological station. More details are provided in the text.

2014 and, on 20 February 2015, a fishing vessel hit the oceanographic buoy and thus temperature, conductivity, and meteorological parameters from the buoy are available only until that date.

Table 2 summarizes data availability and basic statistics for all the instruments except those corresponding to the oceanographic buoy that are presented in Table 3. We decomposed the current measured by all instruments into a parallel (or along shelf-break) and perpendicular (or across shelf-break) components relative to the main direction of the isobaths (37.6 degrees from the north). Data collected within the CASSIS project at the shelf-break that are used in this work are available in Saraceno et al. (2017).

2.1.2. Historical Data

We used all the historical hydrographic data obtained from conductivity-temperature-depth (CTD) stations over the shelf-break between 39°S and 42°S from the NOAA's National Centers for Environmental Information World Ocean Database 2013 available at http://www.nodc.noaa.gov (Boyer et al., 2013) and from two full-depth CTD casts made by R/V Hesperides A-33 on the 10 March 2015 within 1 nautical mile of M1 and M2. We also used underway currents as measured by Hesperides vessel-mounted 75 kHz ADCP (or ship ADCP, SADCP) from the surface to 800 m depth and from moorings that were deployed in the shelf-break region during 1993–1995 (Provost et al., 2017a) and 2001–2003 (Provost et al., 2017b).

Table 2
Statistics of Current Meters and CT Sensors Measurements Over the Continental Patagonian Shelf-Break From December 2014 to November 2015

Mooring name	A4	A4	A4	A4	M11	M12	M13	M21	M22	M23	M24	M31
Depth (m)	305	521	761	977	377	823	1,107	509	951	1,265	1,663	125
Days	337	337	337	337	338	338	338	338	338	338	338	42
θ				3.01	4.2	3.1	2.7	3.4	2.8	2.6	2.4	6.9
$\sigma\theta$				0.2	0.6	0.4	0.2	0.6	0.3	0.2	0.1	4.2
θsM				2.9	3.8	2.8	2.6	2.9	2.6	2.4	2.3	
θwM				3.1	4.7	3.5	2.9	3.9	3.1	2.7	2.3	6.9
S				34.25		34.23	34.36	34.19	34.35	34.62	34.65	
σS				0.06		0.08	0.08	0.05	0.11	0.08	0.03	
SsM				34.28		34.30	34.41	34.20	34.46	34.56	34.59	
SwM				34.22		34.16	34.29	34.13	34.27	34.43	34.60	
P				24.29		27.27	27.41	27.20	27.42	27.55	27.65	
ρsM				27.33		27.35	27.46	27.26	27.50	27.60	27.65	
ρwM				27.27		27.18	27.34	27.11	27.31	27.47	27.65	
V_{max}	82.4	72.4	50.5	44.6	79.7	50.8	46.9	76.8	54.6	46.2	38.5	
V_{max} sM	82.4	72.4	50.5	44.6	79.7	50.8	46.2	61.9	49.3	33.4	27.2	
V_{max} wM	53.5	53.7	48.7	41.1	61.6	42.0	46.9	76.8	54.6	46.2	38.5	49.0
V	35.5	30.5	19.4	12.7	33.9	21.3	14.5	26.6	19.2	12.2	6.0	10.6
VsM MC	52.7	46.4	29.2	16.2	51.3	33.1	22.9	32.8	24.1	16.2	6.2	
VwM	16.9	13.7	9.2	8.7	11.0	6.6	4.8	22.1	13.5	6.8	5.2	10.6
α	35.0	34.4	35.6	44.6	47.2	50.3	40.2	44.8	54.0	65.9	46.0	121.7
αsM	35.1	34.5	35.3	43.2	49.9	49.8	47.9	24.7	41.1	57.2	42.3	
αwM	32.1	30.7	33.2	46.7	46.5	53.8	49.2	80.8	83.0	91.9	48.2	121.7
V||	35.4	28.4	19.4	12.6	33.7	20.8	14.5	26.4	18.5	10.8	6.0	1.1
σV||	23.8	21.0	15.4	9.9	24.7	17.0	13.3	19.8	13.4	11.2	8.1	10.8
V|| sM	52.7	43.5	29.2	16.1	51.3	32.6	23.0	32.0	24.1	15.3	6.2	0.8
σV|| sM	16.4	13.8	10.6	9.1	8.7	8.1	7.5	7.7	8.7	7.7	7.1	6.9
V|| wM	16.8	12.6	9.2	8.6	10.9	6.3	4.7	16.1	9.5	4.0	5.1	1.0
σV|| wM	14.0	13.6	12.5	9.5	20.3	14.5	12.1	25.3	13.9	11.9	8.5	20.4
$V_\perp$	−1.6	−1.6	−0.7	1.5	3.1	4.7	0.7	3.4	5.4	5.8	0.9	10.5
$\sigma V_\perp$	10.2	8.5	6.0	3.9	11.8	8.1	5.3	17.8	9.9	7.8	5.4	12.0
$V_\perp$ sM	−2.3	−2.2	−1.6	4.6	2.3	5.9	0.5	−7.3	1.5	5.4	0.5	6.5
$\sigma V_\perp$ sM	8.5	6.3	3.2	3.2	9.0	5.5	3.1	10.0	5.2	4.6	4.9	8.0
$V_\perp$ wM	−1.6	−1.7	−0.7	1.4	1.1	1.8	1.0	15.1	9.6	5.5	1.0	28.7
$\sigma V_\perp$ wM	11.7	10.0	7.7	4.8	12.8	9.8	7.0	17.2	12.6	10.6	5.9	8.1

Note. Mij denotes current meters and CT sensors at moorings, i being the mooring number and j standing for the level from the surface (see Figure 2). θ (°C) is the potential temperature, S is the salinity, ρ is the potential density (kg m^3), α is the angle in degrees of mean velocity direction relative to the geographical north, V (cm s^{-1}) is the modulus of the time-average velocity and V|| (cm s^{-1}) and $V_\perp$ (cm s^{-1}) are the velocity components along and across the main direction of the isobaths, σ is the standard deviation and unless otherwise specified, and mean values are indicated. Depth is indicated in m. We refer to the strong and weak Malvinas periods as "sM" and "wM."

2.2. Satellite Data

Sea surface temperature (SST) images from Aqua/MODIS were used in the analysis. In order to reduce the frequent cloud cover in the study area, 8 day composites and 4 km spatial resolution standard mapped products available through Ocean Color FTP server were used (http://oceancolor.gsfc.nasa.gov). Geostrophic velocities derived from satellite altimetry maps of absolute dynamic topography (MADT) were obtained for the period 2014–2015. MADT were obtained from the Copernicus Marine Environment Monitoring Service (CMEMS, http://marine.copernicus.eu). The MADT product used in the analysis is based on all available satellites (all-sat). During the period corresponding to the in situ measurement four satellites were available to construct the MADT, ensuring that mesoscale features can be resolved (e.g., Pascual et al., 2006). MADT maps have a daily sampling and a spacing of 1/4 degree in a Cartesian regular grid.

2.3. Methods and In Situ Data Calibration

2.3.1. Currents From Upward-Looking ADCP at A4

The upward-looking ADCP at A4, moored at 1,010 m depth, was configured to operate on 25 m bins. Hence, a total of 40 bins were set to obtain velocity data through the entire water column. Basic statistics of the A4

Table 3
Statistics of ADCP and CT Sensors Measurements Obtained by the Oceanographic Buoy (See Location in Figure 1)

Mooring	B1	B2	B3	B4	B5	B6	C1	C2	C3	C4
Depth	1	10	20	30	50	100	40	80	140	180
Days	62	62	62	62	62	62	42	42	42	42
T	14.6	13.4	11.6	9.3	6.7	5.8				
σT	1.9	1.9	1.9	1.9	0.5	0.2				
S	33.71	33.83	33.84	33.88	33.88	33.91				
σS	0.11	0.11	0.12	0.11	0.11	0.12				
V_{max}							35.9	37.5	31.8	13.3
V							17.7	17.3	11.4	2.8
θ							35.8	37.9	28.4	21.6
V||							17.6	17.2	11.4	2.8
σV||							10.2	9.1	9.0	3.2
$V_{\perp}$							1.8	1.8	−0.6	0.2
$\sigma V_{\perp}$							4.3	3.7	3.2	1.5

Note. B*i* and C*i* denote CT sensors and ADCP measurements, *i* denotes the level measured from the surface. Here T (°C) is temperature, S is salinity, θ is the mean velocity direction (relative to the geographical north), V (cm s^{-1}) is the modulus of the time-average velocity and V|| (cm s^{-1}) and $V_{\perp}$ (cm s^{-1}) are the velocity components along and orthogonal to the isobaths, σ is the standard deviation and unless otherwise specified, mean values are indicated.

currents for the deepest level (bin 1, 977 m) and three shallower levels selected between the 2 and the 29 bin are summarized in Table 2. Comparison of the Hesperide's SADCP with the corresponding profile obtained by the ADCP at A4 (supporting information Figure A1) shows good agreement between the two instruments (rmsd 6.5 cm/s) for the 10 March 2015 between 977 and 89 m. Between 281 and 89 m depth, i.e., between bins 30 and 38, there is a large number of missing data both in the u and v components measured by the ADCP at A4 (supporting information Figure A2a). Missing data in this portion of the water column are recurrent, in particular, in the period from mid-April 2015 to mid-September 2015 (Figure 3a). As it will be discussed later, this period of time is associated with a decrease in current intensity and corresponds to the presence of warmer and less salty waters in comparison to the remaining of the observation record, which presented a stronger MC. The amount of missing data during the weak Malvinas period between 89 and 281 m depth is as large as 65% of the full record, while during strong Malvinas less than 4% of the data are missing in the entire water column (supporting information Figure A2a). Finally, currents measured at bins 39 and 40 (65 and 41 m depth) do not have missing values but the velocity values are largely overestimated, as observed on 10 March 2015 when comparing data with the SADCP from Hesperides (supporting information Figure A1). We do not considered values from bins 39 and 40 in the following.

2.3.2. Potential Temperature and Salinity

θ and S data were first compared with those obtained by R/V Hesperides and then adjusted for the vertical displacements suffered by the tall moorings.

2.3.2.1. Comparison With Hesperides CTD

T and S data at A4, M1 and M2 were compared with two full-depth T and S profiles obtained by R/V Hesperides A-33 on the 10 March 2015 within 1 nautical mile of M1 and M2 mooring. A4 T and S data were compared with the CTD values obtained at the same depth in the profile obtained near M1, located only 21.5 km from M1. T differences between Hesperides CTD moorings are less than 0.08°C for all the instruments. S data from M23 and M24 are larger than those recorded by the Hesperides CTDs by 0.13 and 0.05, respectively. We attribute the difference to a poor calibration of the CT conductivity sensors. The difference is thus subtracted from all the M22 and M23 salinity data. S differences between all other instruments at A4, M2, and M1, and the Hesperides CTD were lower than 0.02 and therefore no correction was applied to the data collected by the moorings (supporting information Figure A3).

2.3.2.2. Adjustment for Vertical Displacements

Vertical displacements of the T and conductivity sensors installed in the tall moorings induce spurious signal in the analysis of θ and S changes. To monitor precisely the vertical displacements, all CT sensors in the tall moorings were equipped with pressure sensors. Large pressure changes during the measurement period on tall moorings are due to mooring motion caused by variations in current velocity. In general, the stronger the MC, the greater the pressure fluctuations. The largest displacements occurred at mooring M1:

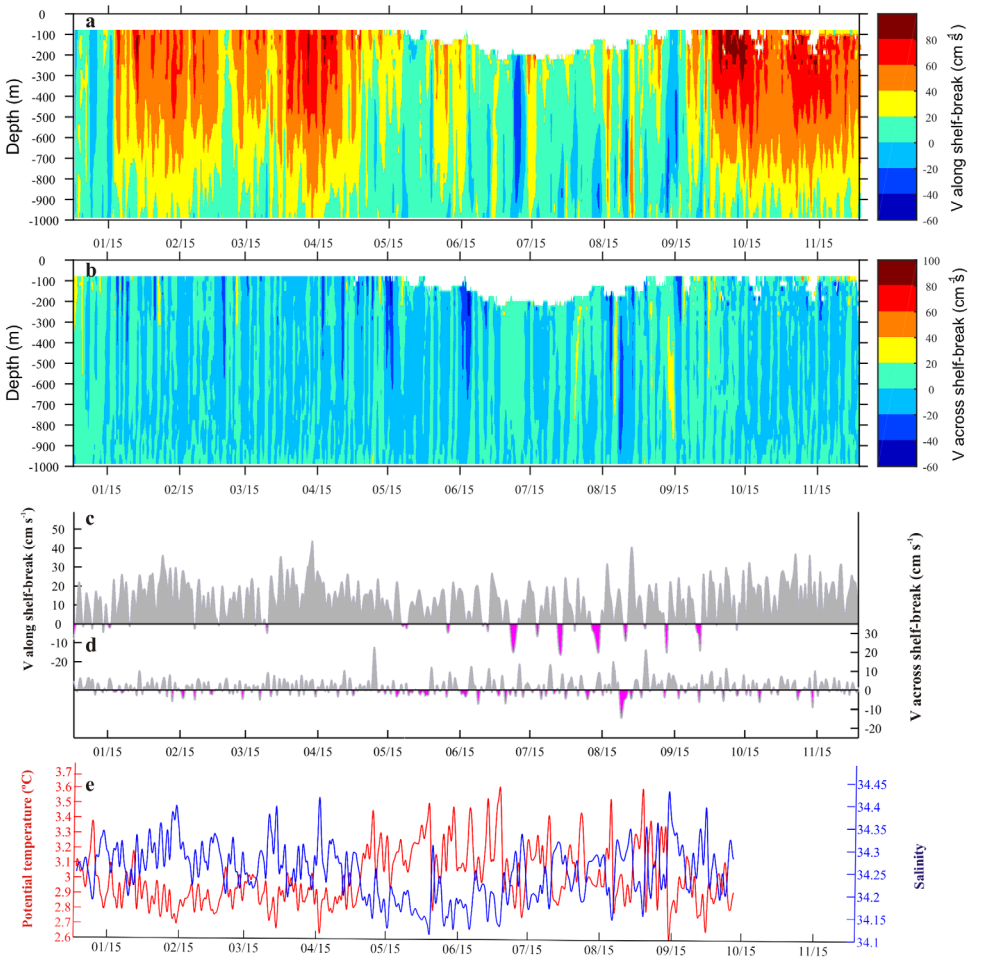

Figure 3. (a) **V** along shelf-break and (b) **V** across shelf-break from ADCP on mooring A4. In situ time series of (c) **V** along and (d) **V** across shelf-break from ADCP at 977 m depth, (e) θ and salinity, at A4 mooring at 1,010 m.

amplitudes as large as 120 db were recorded by the uppermost instruments at M1 during periods when the velocity is larger than 70 cm s^{-1} (supporting information Figure A4). As expected, pressure oscillations were smaller at greater depth. At M1, the pressure records suddenly increased by 20 dbar on 20 June 2015 in the three instruments (M11, M12, and M13; supporting information Figure A4, Figure 4, and supporting information Figure A5, respectively). The pressure was larger until the end of the record despite of the very different flow direction and intensities the mooring was exposed to. The increased pressures thus indicate that the mooring slid to deeper waters. This pressure increase did not produce noticeable changes in the θ and S observations (supporting information Figure A4, Figure 4, and supporting information Figure A5, respectively).

To compensate the changes in θ and S due to large vertical displacements, we applied the method described in Piola (1983) to the measurements of each instrument in M1 and M2:

1. We selected historical T and S values (see section 2.1) within 100 km in the along shelf-break direction and 17 km in the across shelf-break direction from each mooring.
2. The T and S values selected in (i) were used to compute vertical θ and S gradients by means of least square fit.
3. A time series of depth anomalies was computed as the difference between the depth recorded at each time and the shallowest recorded depth.
4. The differences in θ and S values are obtained by multiplying the θ and S gradients obtained in (ii) by the estimated depth anomaly.
5. The corrected θ and S are obtained by adding the differences obtained in (iv).

In the above-described methodology, depth has been estimated from absolute pressure and average density (Tomczak & Godfrey, 1994).

2.3.3. Tide Filtering

All variables (P, θ, S, u, and v) in the five moorings (oceanographic buoy, A4, M1, M2, and M3) are low-pass filtered with a cut-off period of 48 h to remove tidal and inertial variability. Statistical parameters including mean and standard deviation of all the variables are reported in Tables 2 and 3.

3. Results

Time series of along-slope and across-slope velocities (Ua and Uc), θ, S, and P for moorings A4, M1, and M2 are presented in Figures 3, 4, and in supporting information (Figures A4–A9). All the time series are characterized by multiple periodicities. We first describe the time series obtained and focus on subannual time scales (section 3.1). Time-averaged mean and variance ellipses of the current meters are then presented and compared with mean values reported from previous measurements in section 3.2. Finally, a description of how water mass distribution change during the experiment is presented in section 3.3.

3.1. Time Series Analysis: Subannual Scale

During 2014–2015, at the moorings location, the MC displays two distinct regimes characterized by strong and weak along-slope velocities and very different temperature and salinity mean values (Figures 3, 4, and supporting information Figures A4–A9). Hereafter, we refer to these two periods as "strong Malvinas" and "weak Malvinas" following Ferrari et al. (2017). The strong Malvinas period lasts from early-January to mid-April 2015 and from mid-August to late-November 2015. The weak Malvinas period lasts during December 2014 and from mid-April to mid-August 2015. Below we discuss the changes in the MC behavior based on the analysis of each of the variables recorded during these two periods.

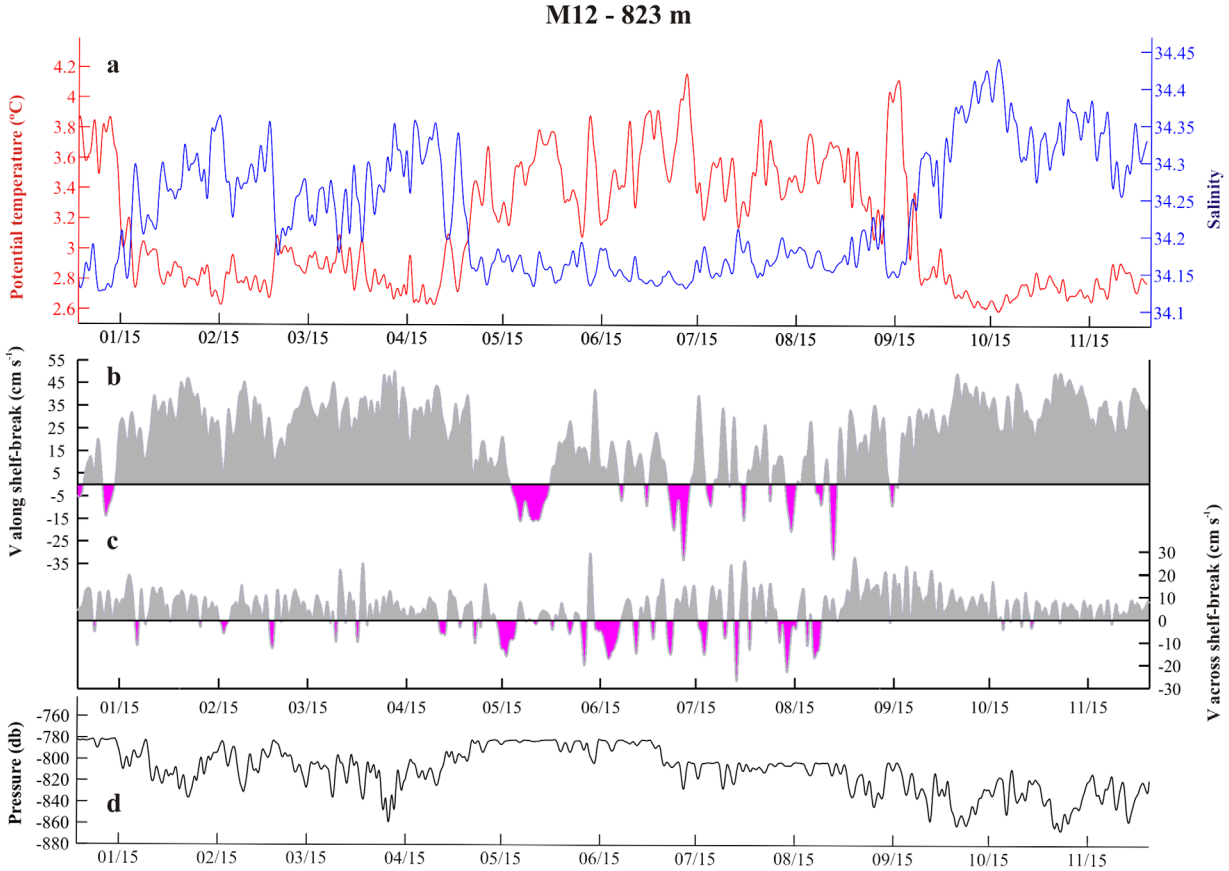

Figure 4. In situ time series of θ and S (a), **V** along (b) and **V** across (c) shelf-break and (d) pressure, at M12 (mean depth 823 m, see also Figure 2).

3.1.1. Along-Slope Currents

During strong MC, along-slope currents (Ua) are always positive for all instruments except for the deepest current meter (M24) that is located at a mean depth of 1,663 m. Reversals of Ua at the shelf-break above 1,600 m are observed only during weak Malvinas periods (Figures 3, 4, and supporting information Figures A4–A8). A comparison of the 2014–2015 currents with the currents observed during the two previous in situ experiments in 1993–1994 (Vivier & Provost, 1999a) and 2001–2003 (Spadone & Provost, 2009) suggests that this is the first time an extended (5 months) period of weak Malvinas is observed. Ua reversals were also observed by Vivier and Provost (1999a) and Spadone and Provost (2009), but only in a few occasions. In the time period analyzed here, the instruments recorded from a minimum of 6 to a maximum of 15 reversals of Ua during the weak MC period (Figures 3, 4, and supporting information Figures A4–A8).

Time and depth averages of Ua are 24, 23, and 15.4 cm s^{-1} for A4, M1, and M2, respectively. The fact that the largest mean value is observed at A4 suggests that the position of the core of the MC is, on average, above the 1,000 m isobaths. The fact that variance ellipses are also more stretched along the major axis at A4 than at M1 and M2 (Figure 5) also suggests that the core of the MC is above the 1,000 m isobaths and that the flow is more parallel to the isobaths there than at M1 and M2. These results are in agreement with the mean SST field (Figure 1a): A4 and M1 are located within the cold tongue that the MC creates flowing northward along the Patagonian shelf-break, while M2 is closer to the eastern edge of such cold tongue.

At A4, the time average of the amplitude of the velocities is remarkably large in the entire water column: mean values range between 35.5 cm/s at 305 m and 12.7 cm/s at 977 m depth. Splitting the time average for the weak and strong regimes shows that during the former Ua is weakened mostly at the surface and thus its vertical shear is almost zero (Table 2 and supporting information Figure A2a). During the strong regime, currents are surface-intensified (Table 2 and supporting information Figure A2b) and the vertical shear is barotropic-equivalent as described in the literature (e.g., Vivier & Provost, 1999b).

3.1.2. Across Shelf-Break Currents (Uc)

During the weak Malvinas period, Uc reversals are more intense at A4 and M1 than at M2 (Figures 3, 4, and supporting information Figures A4–A8), suggesting that larger water mass exchanges between shelf and shelf-break occur under those conditions. At M2, the easternmost mooring that provided a long-term record, the two shallowest current meters show a larger number of Uc reversals during strong Malvinas than during weak Malvinas time period. On the other hand, at M1 and A4, the number of Uc reversals is larger during weak Malvinas than during strong Malvinas. As it will be discussed later, this is very likely a consequence of the deflection of the MC to the East, upstream of the mooring sites, during the weak regime. At A4, the vertical shear of the mean of Uc is close to zero, during both strong and weak Malvinas periods (supporting information Figure A2c).

3.1.3. Potential Temperature and Salinity

All time series of θ and S within all instruments at A4, M1, and M2 are anticorrelated. The amplitude of the oscillations can be quite large: at A4, θ (S) increased (decreased) from 2.6°C (34.41) to 2.9°C (34.23) between 2 April 2015 at 2 PM and 5 April 2015 at 3 AM. Such large changes in θ and S suggest that different water masses can pass over A4 even at short time scales.

Statistics of all the variables recorded at the moorings, including θ and S, reveal significantly different mean values during strong and weak Malvinas (Table 2). During strong Malvinas, θ (S) has lower (higher) values than during weak Malvinas at all instruments except M24. θ and S differences between strong and weak regimes varies according to the depth of the instrument and its location. For example, the mean θ recorded at M11 during strong Malvinas is 3.75°C and increases to 4.71°C during weak Malvinas (Table 2). On the other hand, at M24, θ and S do not show significant differences between

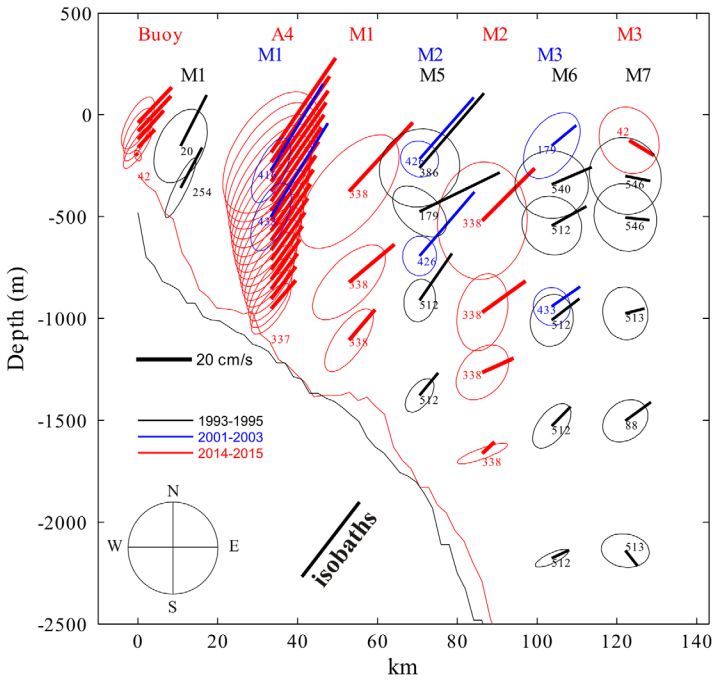

Figure 5. Mean flow and variance ellipses for each current meter along the section: in black from the WOCE time series (1993–1995), in blue from the 2001 to 2003 time series and in red from 2014 to 2015 time series. Number of days with valid data are indicated. The direction of isobaths is indicated by the thick line at bottom left. The topography along the sections where the instruments were deployed is indicated in black (2014–2015 and 1993–1995) and in red (1993–1995). *X* axis is distance along the section in km, the origin being the Buoy (2014–2015) location.

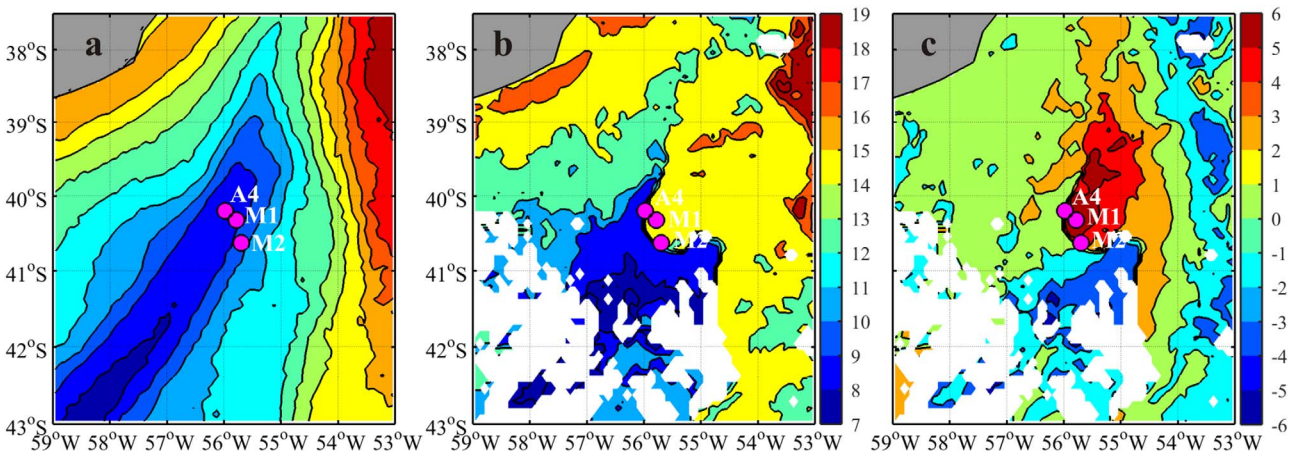

Figure 6. (a) SST climatology calculated by all images obtained during May by MODIS Aqua from 2002 to 2017; (b) SST 8 day average from 9 to 16 May 2015; (c) Difference between plots a and b.

the strong and weak regimes (supporting information Figure A9 and Table 2). This result suggests that the strong and weak regimes alter the thermohaline structure in the water column only above M24, i.e., above 1,600 m depth. As the core of the MC flows in the upper 1,600 m in the shelf-break, it is reasonable to observe the largest changes in the thermohaline structure in the upper 1,600 m of the water column and not below that depth.

One of the largest reversal events of Ua occurred during weak Malvinas, between 10 and 19 May 2015. During that event, the θ at M11 raised from 4.9°C to 7.04°C (supporting information Figure A4). To better understand the regional pattern associated with this event, we computed the SST anomaly (Figure 6c) as the difference between the record-length mean of all images obtained during May by MODIS Aqua (from 2003 to 2017, Figure 6a) and the 8 day SST mean centered on 12 May 2015 (Figure 6b). It is clearly seen that A4 and M2 are very close to a surface frontal region and that M1 is surrounded by warm waters. Yet the whole array is in a region that is under a large (>2°C and up to 6°C) SST anomaly. The image corresponding to the previous 8 day composite clearly suggests that the warm waters are coming from the east (supporting information Figure A10). A week after the event, warm waters moved back eastward (supporting information Figure A10). SST time series at the moorings (supporting information Figure A11) suggest that this event was the only one, for the period December 2014 to November 2015, during which the presence of subtropical water is observed over M1 and M2. The combined analysis of satellite images and in situ data suggests that subtropical waters are present only occasionally over the position of the moorings and affect the uppermost portion of the water column. Indeed, the large increase of potential temperature is observed at M11 at 377 m but not at M21, which mean depth is 509 m.

3.1.4. Covariability of Temperature, Salinity, and Velocity Fields

To obtain the main patterns of space-time variability of θ, S, u, and v, we computed empirical orthogonal functions (EOFs) considering measurements from all instruments that measured during the whole period. We did not consider instruments located at M11 and M31 because of the absent of CT sensors at those average depths (Figure 7 and Table 2). The first two modes of variability considering all variables (θ, S, u, and v) explain 57.6% of the total variance. Here we discuss only mode 1 that explains 45.9% of the total variance. The associated temporal series unequivocally distinguish the strong and weak Malvinas time periods. The first mode of the combined EOF also shows that the θ increases (decreases) during weak (strong) regime, while S decreases (increases). The exception to the above-described pattern occurs at M24. M24 is located at a mean depth of 1,663 m, and, as pointed out in section 3.2, the nature of the variability at this site differs from the one observed in the upper portion of the water column along the continental slope. The amplitudes corresponding to the first EOF of θ and S are larger at M1 and M2 above 1,600 m than at A4 (see colored dots in Figure 7), suggesting that the coupling between θ and S and the strong and weak regimes reflected by mode 1 is more evident at M1 and M2 above 1,600 m than at A4.

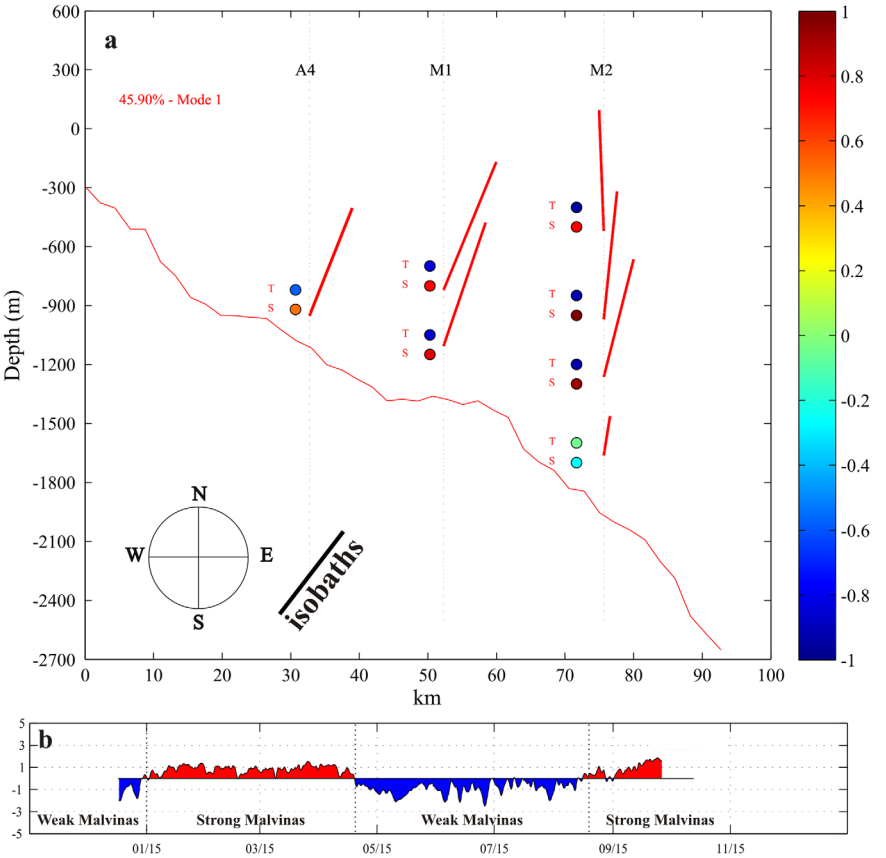

Figure 7. (a) Mode 1 of EOF obtained considering u, v, θ, and S for the CASSIS period (2014–2015). All variables were normalized before computing the EOF. (b) Time series corresponding to mode 1.

3.2. Comparison With Historical Data

3.2.1. Means and Variance Comparison

Figure 5 shows means and variance ellipses of the currents recorded during 2014–2015 within the CASSIS project (Saraceno et al., 2017) and during years 1993–1995 (Provost et al., 2017a) and 2001–2003 (Provost et al., 2017b) in the shelf-break between 40°S and 41°S. In the following, we added the years of the data sets as a subscript of the moorings of the periods 1993–1995 and 2001–2003. Moorings A4, M2, and M3 were located very close to former moorings: $M1_{93-95}$ is close to A4, $M5_{93-95}$ and $M2_{01-03}$ are close to M2, and $M7_{93-95}$ and $M3_{01-03}$ are close to M3 (Figure 1b). Magnitudes of mean velocities from different periods are very similar within neighborhood moorings (Figure 5). Directions of mean velocities are also similar within different observation periods, being always aligned with the local bathymetry, up to 90 km from the buoy. The mean velocities decrease with depth at all moorings during 2014–2015 and in all former moorings in 1993–1995, down to 1,600 m. Mean velocities during 2001–2003 present a very small vertical shear compared to the other two periods (Figure 5).

The direction of the major axes of the variance ellipses is consistent within the different time periods: they are oriented parallel to the isobaths up to 90 km east of the buoy and have a northeast-southwest direction for those located further east (Figure 5). In general, variance ellipses are more stretched in the direction perpendicular to the isobaths up to 60 km east of the buoy (Figure 5). East of that position, the variability in current direction, responsible of the more round-like shape of the variance ellipses, is associated with more intense mesoscale activity.

The magnitude of the variance ellipses is larger during 2014–2015 than during the other measurement periods (Figure 5). This observation is in good agreement with the fact that during 2014–2015 the MC is weak for 5 of the 11 months of measurements. Indeed, during weak Malvinas period along and across shelf-break

currents show larger variability than during the strong Malvinas period (see section 3.2), and neither during 2001–2003 nor during 1993–1995 a weak regime has been observed for so long.

3.2.2. Comparison of Principal Modes of Variability of the Current Velocities

To further compare the velocities obtained during 2014–2015 with those obtained in the two previous observation periods we computed EOFs for each mooring separately. We did not consider moorings whose time series are shorter than 170 days. Results are shown in Figures 8 and 9. The main objective of this analysis is to explore the vertical structure of the flow and to provide an overview of the velocity field variation above the continental slope over the years. The two leading EOFs characterize the circulation in an along-slope mode (EOF||, Figure 8) and an across-slope mode ($EOF_{\perp}$, Figure 9). Their associated time series are used to summarize and discuss the time variability of the MC. The new record shows that EOF|| at A4 and M1 was surface-intensified and a downward clockwise rotation of the horizontal velocity vector below 900 m is evident at M1 (Figure 8a). At M2, the EOF|| also shows that surface currents are more intense but have a more meridional direction compared to M1 and A4 and, at the deepest level, the direction is across-slope. In general, regardless of the year, all vectors above 1,500 m show a direction comparable with the main direction of the isobaths. The only two measurements obtained below 1,500 m, located at M2 and $M7_{93\_95}$ are clearly not parallel to the isobaths, suggesting that different currents are being sampled there.

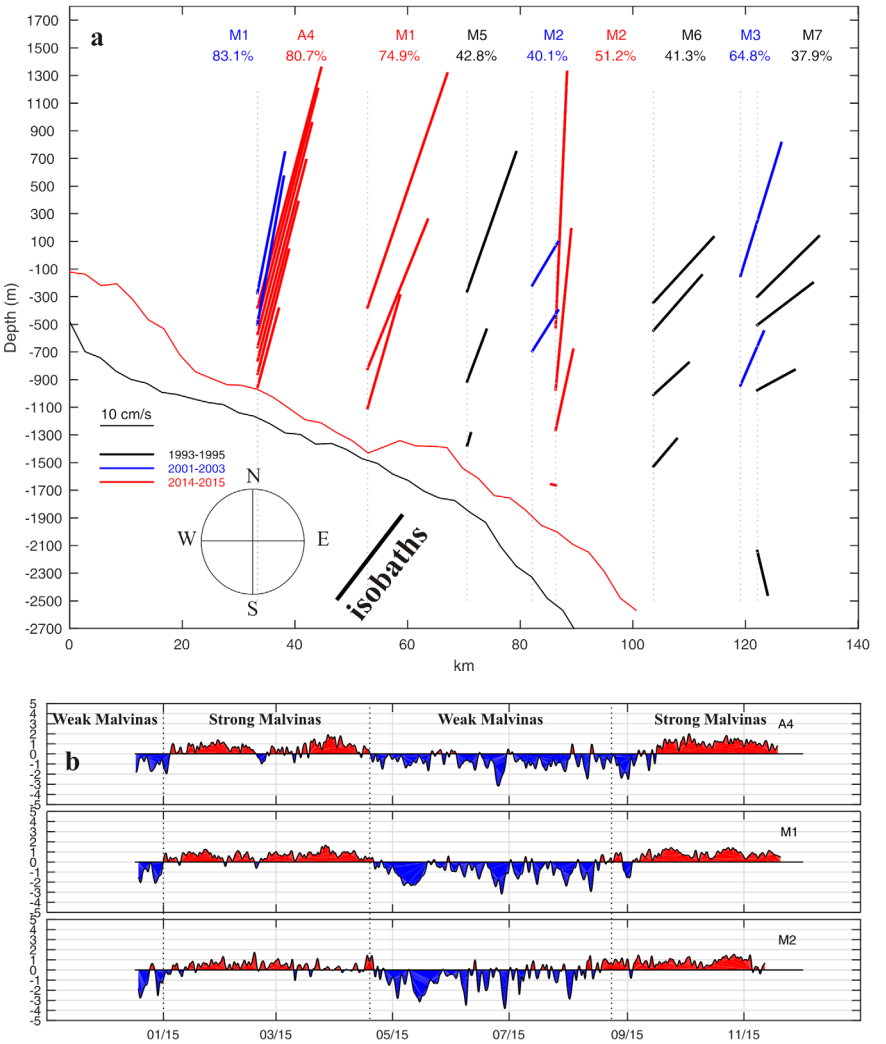

Figure 8. (a) Empirical orthogonal functions oriented along the mean flow (EOF||) with the percentage of total variance explained; in black, from the WOCE time series (1993–1995), in blue, from the CLIVAR time series (2001–2003) and in red from the CASSIS time series (2014–2015). Direction of isobaths is indicated by the thick solid line at bottom left. (b) Time series corresponding to the CASSIS time period.

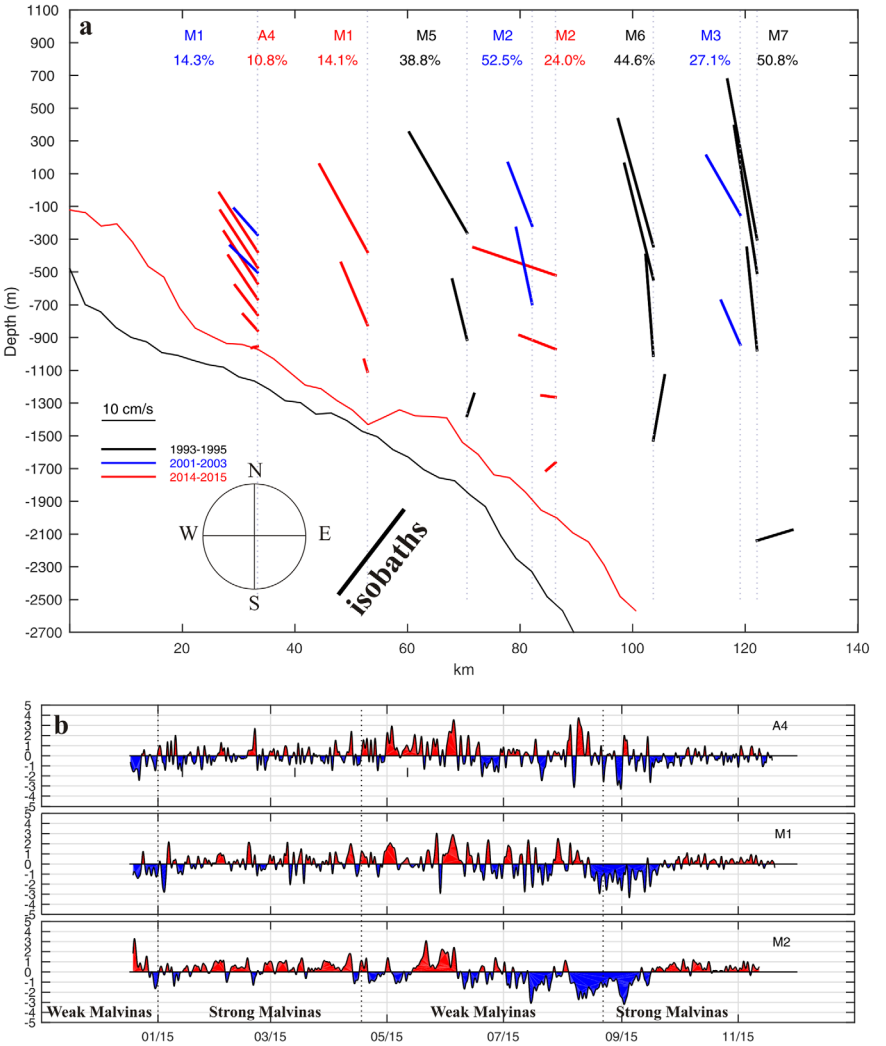

Figure 9. As in Figure 8 for the across-slope component of the mean flow. The time series corresponding to the other periods can be found in Figure 10 paper Vivier and Provost (1999a) and Figure 7b paper Spadone and Provost (2009).

The $EOF_{\perp}$ at A4, M1, and M2 (Figure 9a) shows that the flow direction varies little with depth and, as for EOF|| (Figure 8a), the velocity amplitudes decrease with depth, indicating an equivalent-barotropic vertical structure. The $EOF_{\perp}$ shows similar across-slope directions of the flow in the upper 1,500 m regardless of the year (Figure 9a). Below 1,500 m, the $EOF_{\perp}$ has a downward component.

In agreement with the observation made on the time series of the data (section 3.1), the time series associated to the first two modes of the EOF clearly show the oscillation pattern between the strong and weak regimes (Figure 8b). It is worth observing that this pattern has not been observed previously: the time series corresponding to the along shelf-break variability of the MC for 1993–1995 and 2001–2003 show a regime that is more similar to the strong Malvinas period observed here most of the time, with only sporadic negative events (see Figure 7 in Vivier and Provost (1999a) and Figure 2 in Spadone and Provost (2009)).

The spatial pattern of the across shelf-break variability (Figure 9a) shows that similar results are obtained for the three observation periods. Interestingly, the amplitude of the oscillations of the across-slope mode during weak regime (Figure 9b) is larger than during strong regime. This result is clearly quantified in Table 2: standard deviations of across-slope velocities are significantly larger during weak Malvinas period than during strong Malvinas period (e.g., for M12 $\sigma V_{\perp}$ is 5.5 cm/s during strong regime and is 9.8 cm/s during weak regime). Therefore, more intense exchanges in the across shelf-break direction might be expected during weak Malvinas period.

The percentages of variance explained in the EOF analysis for the different years should be compared with caution since the number of current meters at each mooring in the three different observation periods is different, and thus percentages cannot be directly compared. Only two current meters per mooring were deployed in 2001–2003 and between three and four in 1993–1995 and 2014–2015.

3.3. Water Mass Distribution Changes During 2014–2015

To characterize water masses at the mooring arrays the θ–S diagrams of the data collected at M1, M2, and A4 are plotted together with historical CTD data collected in the vicinity of moorings (Figure 10). Three water masses are recognized: Sub-Antarctic Mode Water (SAMW), Antarctic Intermediate Water (AAIW), and Upper Circumpolar Deep Water (UCDW) (Figures 10a and 10b) according to their properties (see Table 4). θ–S diagrams show that during 2014–2015 SAMW were present only during the weak regime. Furthermore, different water masses are present within the location of each instrument, depending on the period of time considered. In the following we detail where and when each water mass has been found:

- Sub-Antarctic Mode Water

  The lightest waters in the θ–S diagrams collected during 2014–2015 correspond to the fresh and relatively cold SAMW. SAMW were present at M21 only during the weak Malvinas period (Figures 10h and 11d).
- Antarctic Intermediate Water

  During 2014–2015 AAIW is observed in all moorings at different depths. At A4, located in the core of the MC at 976 m depth, the θ–S diagrams display the presence of AAIW both during strong and weak regimes (Figures 10c, 10d, 11c, and 11d). At M1, AAIW appeared during strong and weak regimes in M12, at an intermediate depth of 823 m (Figures 10e, 10f, 11c, and 11d) and only during weak regime at M13 (Figures 10f and 11d). During weak Malvinas period AAIW at M12 is lighter than during strong Malvinas period (Table 2). We found the same pattern at M2: AAIW was observed only at an average depth of 509 m during strong regime (M21, Figures 10g and 11c) and was registered up to 951 m during weak regime (M22, Figures 10h and 11d).
- Upper Circumpolar Deep Water

  UCDW is observed at M13, M22, M23, and M24 during strong and weak regimes. The time average of the density within the instruments located above 1,600 m during weak Malvinas is lighter than during the strong Malvinas (Figures 10e, 10f, 10g, 10h, 11c, 11d, and Table 2). On the other hand, the density does not change at M24, located at 1,663 m (Figures 10g, 10h, 11c, and 11d).

The above observations show that a clear change in the vertical water mass structure occurs in the upper 1,600 m between strong and weak Malvinas periods: water masses deepen and shifted eastward. We further discuss this result in section 4.

4. Discussion and Summary

This work presents the first time series of θ and S data collected in the northern Malvinas Current. Two complementary articles further discuss the results found here, particularly putting the results in a regional context based on the combined analysis of satellite altimetry data (Ferrari et al., 2017) and computing and analyzing the MC transport (Artana et al., 2018). The time series reported here revealed the changes in the structure of the water masses and how they relate with changes in the currents during 338 days. The current meter observations show that, in agreement with previous reports (Spadone & Provost, 2009; Vivier & Provost, 1999a), the mean flow of the MC is parallel to the direction of the isobaths. At subannual time scales, we observed that changes in θ and S are associated with changes in the intensity of the along-isobath flow. We identified two distinct periods based on the current intensity, referred to as "strong Malvinas" and "weak Malvinas." During strong Malvinas period, the mean θ (S) is lower (higher) than during weak Malvinas period. θ-S diagrams showed that different water masses were sampled at the moorings during the strong and weak regimes. To understand the nature of these fluctuations, it is useful to analyze the satellite SST and altimetry data. During the weak Malvinas period (see Figure 11b), the MC deflected offshore just upstream of the mooring site. Consequently, at that time, the MC along-slope velocities decreased at the position of the moorings. SST images and geostrophic velocities derived from satellite altimetry clearly

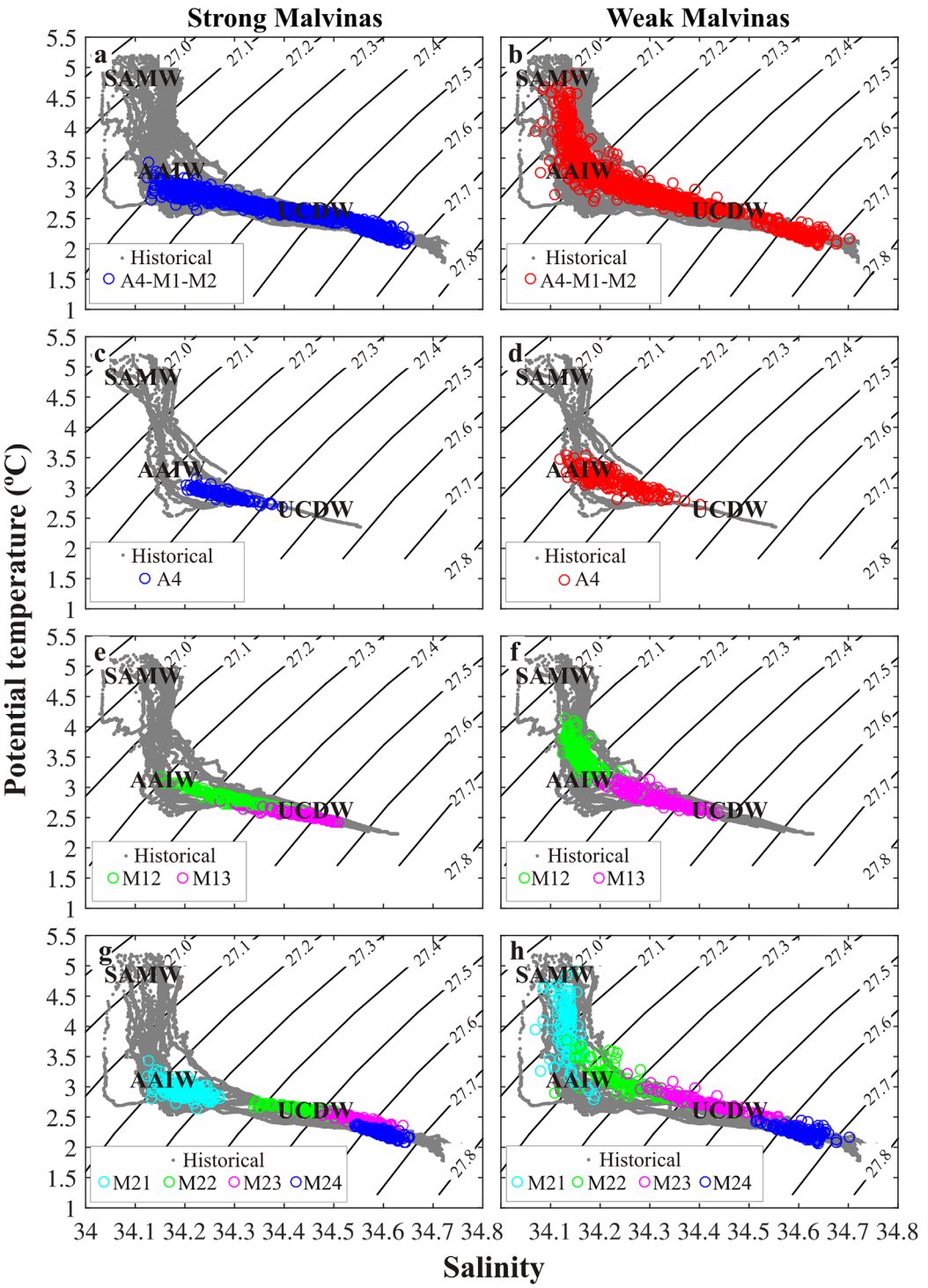

Figure 10. θ-S data collected by instruments at moorings A4, M1, and M2. Grey crosses show historical CTD data collected in the region near moorings location. Constant potential density lines are displayed in black. (a) θ-S data collected by instruments during the strong regime (blue crosses) and historical data; (b) θ-S data collected by instruments during the weak regime (red crosses) and historical data; (c) θ-S data collected: by A4 at 1,010 during the strong and (d) the weak regimes; (e) M12 and M13 during the strong and (f) the weak regimes; and by M21, M22, M23, and M24 during the strong (g) and the weak regimes (h). See Figure 2 for the vertical location of the instruments.

Table 4
Values of θ, S, and ρ Used to Classify Water Masses From the Nomenclature Described by Piola and Gordon (1989), Stramma and England (1999), and Maamaatuaiahutapu et al. (1999)

Water mass	θ	S	ρ
SAMW	>3.5	<34.2	26.8–27.05
AAIW	2.9–3.5	34.1–34.2	27.05–27.25
UCDW	<2.9	>34.2	27.25–27.80

show the presence of warm waters derived from the Brazil Current close to the location of the moorings during the weak Malvinas period. These warm waters appear to obstruct the northward penetration of the MC and force it to veer southeastward (Figure 11b). In contrast, during strong Malvinas period sub-Antarctic waters pass through the mooring array and penetrate almost 1.5° further north (Figure 11a). SST upstream and downstream of the mooring locations are the same during strong Malvinas period whereas the SST increase ~4°C just north of the moorings during weak Malvinas period due to the approach of warmer waters.

Satellite altimeter-derived geostrophic velocities are significantly correlated with 20 day low-pass filtered current meter observations and corroborate the weak and strong regimes reported here (Ferrari et al., 2017). Ferrari et al. (2017) showed that the first two modes of variability explain up to 41% of the variance of sea-level anomaly around the mooring location. The first mode represents meridional migrations in the penetration of the MC, while the second mode represents zonal displacements of the Brazil Current overshoot (Ferrari et al., 2017). Both modes are associated with standing waves in the northern Argentine Basin, yet the forcing mechanism of such waves is still unclear (Ferrari et al., 2017).

Combining satellite altimetry and in situ data, Artana et al. (2018) showed that the transport of the MC at the mooring location presents large fluctuations between December 2014 and November 2015. As

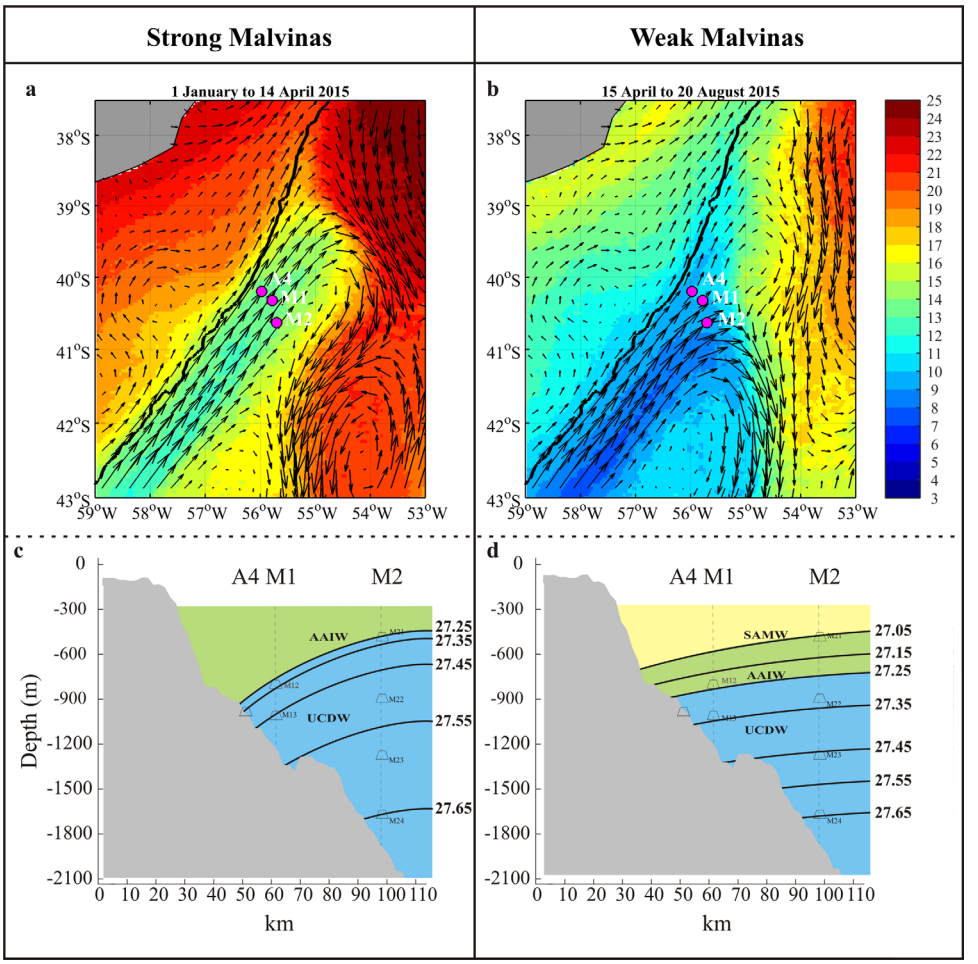

Figure 11. SST (background color) and geostrophic velocities (black arrows) averaged for the (a) strong and (b) weak Malvinas period. Black contour in Figures 11a and 11b corresponds to the 200 m isobaths. Magenta dots represent the position of the instruments. Water masses scheme during (c) the strong and (d) the weak regimes from potential density data.

expected, during the strong regime, the MC transport has larger values than during the weak regime. The 24 year transport time series shows that during December 2014–November 2015 a relatively small mean value (31.7 Sv compared with 37.1 Sv for 24 years) and a substantially larger standard deviation (9.8 Sv versus 6.6 Sv over 24 years) are obtained (Artana et al., 2018). These changes reflect the large variability observed during 2014–2015 when the moorings were deployed.

The weak regime is associated with a change of the potential temperature and salinity structure of the water column on the shelf-break. Furthermore, positive SST anomalies (>4°C) are observed during the weak regime over a large region located northeast of the array (supporting information Figure A12). This SST anomaly could affect air-sea heat fluxes in the region. A recent work showed that mesoscale features impact the sensible and latent heat flux, affecting the net heat exchange at the air-sea interface (Leyba et al., 2017). Therefore, a local climate impact could be expected when conditions similar to the one observed during the weak regime occur.

Distinct vertical structure of the water masses in the upper 1,600 m are associated with strong and weak Malvinas periods (Figures 10, 11c, and 11d). During strong Malvinas period, AAIW and UCDW occupy most of the waters spanning the mooring array (Figures 10a, 10c, 10e, 10g, and 11c). During the weak Malvinas period, SAMW are observed at 509 m (Figures 10h and 11d) and AAIW and UCDW deepen and shift eastward relative to their position during strong Malvinas. Mesoscale process is probably at the origin of the deepening of the water masses during the weak Malvinas period as suggested by Maamaatuaiahutapu et al. (1999) to explain the presence of SAMW at a depth of 800 m north of 38°S. In turn, eddy kinetic energy mesoscale process is stronger during the weak Malvinas period (Ferrari et al., 2017) and thus intrusions of subtropical waters associated with intense mesoscale variability may favor the deepening of the water masses.

The ADCP observations at A4 also offer an excellent opportunity to compare satellite-derived geostrophic velocities with in situ currents. Ferrari et al. (2017) showed that geostrophic velocities computed from gridded data represent in situ velocity better than along-track data. Here we show that gridded altimetry data represent adequately (rmsd ~12 cm/s) in situ currents both for the strong and weak Malvinas periods between 200 and 500 m (supporting information Figure A2a). Below 500 m rmsd increases downward up to 28 cm/s during the strong Malvinas period and remains constant at 12 cm/s during the weak Malvinas period. To explain this difference, we plotted the mean vertical profile of Ua and Uc during weak and strong Malvinas periods (supporting information Figures A2b and A2c). Mean Uc between 200 and 1,000 m are almost identical during weak and strong regimes (supporting information Figure A2c). On the other hand, mean Ua during the weak regime presents almost no difference between 200 and 1,000 m while during the strong regime shows a large vertical shear, in particular between 500 and 1,000 m depth (supporting information Figure A2b). Thus, during the weak regime, the MC is weakened mostly in the upper 1,000 m, and its vertical shear is almost zero. During the strong regime, a barotropic-equivalent structure is observed: currents are intensified above 1,000 m. At the same time, the largest Ua vertical gradient between 500 and 1,000 m during the strong regime leads to the increased difference observed between altimeter and in situ within that depth range. The above observations show that the vertical structure of the water column is critical to use satellite altimetry as a proxy of subsurface currents, even under mostly baroclinic conditions such as those within the MC.

Finally, this study shows that large anomalies in SST are observed during the weak regime, north of the moorings. The impact that such anomalies might have through air-sea heat fluxes in the local climate of the region will be the subject of future studies. As the Brazil-Malvinas Confluence region has large concentrations of chlorophyll-a year-round (Saraceno et al., 2005) it is also expected that large anomalies as the one observed during the weak regime might affect the chlorophyll-a distribution and its associated primary production.

Acknowledgments

A large number of people helped collecting the in situ data that are the core of the results presented here. We particularly thank the support of the following institutions: SHN, Mincyt, INIDEP, CONICET, UBA, Prefectura Naval Argentina, Puerto Deseado crew, CNRS, Sorbonne Université LOCEAN, LOPS, and DT-INSU. This study is a contribution to EUMETSAT/CNES DSP/OT/07-2118 and DSP/OT/07-4571, CONICET-FYPF PIO 133-20130100242. Additional support was provided by grant CRN3070 from the Inter-American Institute for Global Change Research through NSF grant GEO-1128040. We acknowledge support from the MINCYT-ECOS-Sud A14U0 project in facilitating scientific exchanges between Argentina and France. Data from R/V Hespérides were collected in the framework of cruise TIC-MOC, as part of the project CTM2011–28867 funded by the Spanish government. G.F.P. and L.S.L. benefited from scholarships from CONICET, Argentina. The satellite data are available at Copernicus Marine Environment monitoring service (CMEMS) (http://marine.copernicus.eu/) and the in situ data are available at SEANOE (www.seanoe.org cf. references below Provost et al., 2017a, 2017b; Saraceno et al., 2017) and at the NOAA's National Centers for Environmental Information World Ocean Database 2013 (http://www.nodc.noaa.gov cf. references below Boyer et al., 2013).

References

Acha, E. M., Mianzan, H. W., Guerrero, R. A., Favero, M., & Bava, J. (2004). Marine fronts at the continental shelves of austral South America—Physical and ecological processes. *Journal of Marine Systems*, *44*, 83–105. https://doi.org/10.1016/j.jmarsys.2003.09.005

Artana, C., Ferrari, R., Koening, Z., Sennechael, N., Saraceno, M., Piola, A. R., et al. (2018). Malvinas Current volume transport at 41°S: A 24-year long time series consistent with mooring data from 3 decades and satellite altimetry. *Journal of Geophysical Research: Oceans*, *123*, 378–398. https://doi.org/10.1002/2017JC013600

Boyer, T. P., Antonov, J. I., Baranova, O. K., Coleman, C., García, H. E., Grodsky, A., et al. (2013). *World Ocean Database 2013* (*NOAA Atlas*(72), 209 p.). Silver Spring, MD: National Oceanic and Atmospheric Administration. https://doi.org/10.7289/V5NZ85MT

Bryden, H. L. (1973). New polynomials for thermal expansion, adiabatic temperature gradient and potential temperature of sea water. *Deep Sea Research and Oceanographic Abstracts*, *20*, 401–408. https://doi.org/10.1016/0011-7471(73)90063-6

Ferrari, R., Artana, C., Saraceno, M., Piola, A. R., & Provost, C. (2017). Satellite altimetry and current-meter velocities in the Malvinas Current at 41°S: Comparisons and modes of variations. *Journal of Geophysical Research: Oceans*, *122*, 9572–9590. https://doi.org/10.1002/2017JC013340

Garzoli, S. L., & Matano, R. (2011). The South Atlantic and the Atlantic meridional overturning circulation. *Deep-Sea Research Part II*, *58*, 1837–1847. https://doi.org/10.1016/j.dsr2.2010.10.063

Gordon, A. L. (1981). South Atlantic thermocline ventilation. *Deep-Sea Research Part A*, *28*, 1239–1264. https://doi.org/10.1016/0198-149(81)90033-9

Leyba, I. M., Saraceno, M., & Solman, S. A. (2017). Air-sea heat fluxes associated to mesoscale eddies in the Southwestern Atlantic Ocean and their dependence on different regional conditions. *Climate Dynamics*, *49*, 2491–2501. https://doi.org/10.1007/s00382-016-3460-5

Maamaatuaiahutapu, K., Garçon, V. C., Provost, C., Boulahdid, M., & Bianchi, A. A. (1994). Spring and winter water mass composition in the Brazil-Malvinas Confluence. *Journal of Marine Research*, *52*, 397–426. https://doi.org/10.1357/0022240943077064

Maamaatuaiahutapu, K., Provost, C., Andrié, C., & Vigan, X. (1999). Origin and ages of mode waters in the Brazil-Malvinas Confluence region during austral winter 1994. *Journal of Geophysical Research*, *104*, 21051–21061.

Matano, R. P., & Palma, E. D. (2008). On the upwelling of downwelling currents. *Journal of Physical Oceanography*, *38*, 2482–2500. https://doi.org/10.1175/2008JPO3783.1

McCartney, M. S. (1977). Subantarctic mode water *in a voyage of discovery*. *Deep-Sea Research*, *24*, 103–119.

McCartney, M. S. (1982). The subtropical recirculation of mode waters. *Journal of Marine Reearch*, *40*, 427–464.

Miller, R. N., Matano, R. P., & Palma, E. D. (2011). Shelfbreak upwelling induced by alongshore currents: Analytical and numerical results. *Journal of Fluid Mechanics*, *686*, 239–249.

Piola, A. R. (1983). Horizontal advection of temperature in the Drake Passage. *Journal of Geophysical Research*, *88*, 7634–7640.

Piola, A. R., & Gordon, A. L. (1989). Intermediate waters of the western South Atlantic. *Deep-Sea Research*, *36*, 1–16.

Piola, A. R., & Matano, R. P. (2001). Brazil and Falklands (Malvinas) currents. In J. H. Steele, S. A. Thorpe, & K. K. Turekian, (Eds.), *Encyclopedia of ocean sciences* (pp. 340–349). London, UK: Academic Press.

Provost, C., Lanoiselle, J., Kartavtseff, A., Spadone, A., Artana, C., & Durand, I. (2017b). *Malvinas Current 2001–2003: Mooring velocities*. SEANOE. Retrieved from www.seanoe.org https://doi.org/10.17882/51479

Provost, C., Lanoiselle, J., Kartavtseff, A., Vivier, F., Artana, C., & Durand, I. (2017a). *Malvinas Current 1993–1995: Mooring velocities*. SEANOE. Retrieved from www.seanoe.org https://doi.org/10.17882/51483

Romero, S. I., Piola, A. R., Charo, M., & Garcia, C. A. E. (2006). Chlorophyll-a variability off Patagonia based on SeaWiFS data. *Journal of Geophysical Research*, *111*, C05021. https://doi.org/10.1029/2005JC003244

Saraceno, M., Guerrero, R., Piola, A. R., Provost, C., Perault, F., Ferrari, R., et al. (2017). *Malvinas Current 2014–2015: Mooring velocities*. SEANOE. https://doi.org/10.17882/51492

Saraceno, M., Provost, C., & Piola, A. R. (2005). On the relationship between satellite-retrieved surface temperature fronts and chlorophyll a in the western South Atlantic. *Journal of Geophysical Research*, *110*, C11016. https://doi.org/10.1029/2004JC002736

Spadone, A., & Provost, C. (2009). Variations in the Malvinas Current volume transport since October 1992. *Journal of Geophysical Research*, *114*, C02002. https://doi.org/10.1029/2008JC004882

Stramma, L., & England, M. (1999). On the water masses and mean circulation of the South Atlantic Ocean. *Journal of Geophysical Research*, *104*, 20863–20883.

Talley, L. D. (1996). Antarctic Intermediate Water in the South Atlantic. In *The South Atlantic* (pp. 219–238). Berlin, Heidelberg: Springer. https://doi.org/10.1007/978-3-642-80353-6_11

Tomczak, M., & Godfrey, J. S. (1994). *Regional oceanography: An introduction*. Oxford, UK: Pergamon.

Vivier, F., & Provost, C. (1999a). Direct velocity measurements in the Malvinas Current. *Journal of Geophysical Research*, *104*, 21,083–21,104.

Vivier, F., & Provost, C. (1999b). Volume transport of the Malvinas Current: Can the flow be monitored by TOPEX/POSEIDON? *Journal of Geophysical Research*, *104*, 21,105–21,122.